ELSEVIER

Journal of Nuclear Materials 244 (1997) 185–194

journal of nuclear materials

Energetics of formation and migration of self-interstitials and self-interstitial clusters in α-iron

B.D. Wirth [a,*], G.R. Odette [a,c], D. Maroudas [b], G.E. Lucas [a,b]

[a] *Department of Mechanical Engineering, University of California, Santa Barbara, CA 93106 USA*
[b] *Department of Chemical Engineering, University of California, Santa Barbara, CA 93106 USA*
[c] *Department of Materials, University of California, Santa Barbara, CA 93106 USA*

Received 26 July 1996; accepted 2 October 1996

Abstract

Energetic primary recoil atoms from fast neutron irradiation generate both isolated point defects and clusters of vacancies and interstitials. Self-interstitial mobility as well as defect cluster stability and mobility play key roles in the subsequent fate of defects and, hence, in the overall microstructural evolution under irradiation. Self-interstitials and two, three and four-member self-interstitial clusters are highly mobile at low temperatures as observed in molecular-dynamics simulations and high mobility probably also extends to larger clusters. In this study, the morphology, energetics and mobility of self-interstitials and small self-interstitial clusters in α-iron are studied by molecular-statics and molecular-dynamics simulations using a Finnis–Sinclair many-body interatomic potential. Self-interstitial migration is found to be a two-step process consisting of a rotation out of the $<110>$ split-dumbbell configuration into the $<111>$ split-dumbbell configuration and $<111>$ translational jumps through the crowdion configuration before returning to the $<110>$ dumbbell configuration. Self-interstitial clusters of $<111>$ type split-interstitials assembled on adjacent {110} planes migrate along $<111>$ directions in an amoeba-like fashion by sequential local dissociation and re-association processes.

1. Introduction

It is well established that the neutron irradiation embrittlement of nuclear reactor pressure vessels derives from the formation of an ultra-fine-scale microstructure [1] [1–3]. In manganese-molybdenum pressure vessel steels containing copper, the predominant feature is the formation of copper-rich precipitates [4–6]. The primary source for the formation of such ultra-fine-scale features is the highly supersaturated concentrations of point defects and point-defect clusters created in neutron-induced displacement cascades. The excess point defect fluxes are responsible for the rearrangement of solute impurities via radiation-enhanced diffusion and/or radiation-induced segregation leading to the formation of second phases either in or out of thermodynamic equilibrium. A large number of defect-solute complexes, which evolve on the nanometer scale, are also possible. Such features impede dislocation glide, thereby resulting in radiation hardening and embrittlement.

Numerous theoretical studies and molecular-dynamics simulations have been performed on displacement cascade evolution and the general characteristics of the cascade are quite well established [7–10]. A displacement cascade in α-iron produces a vacancy rich core surrounded by a shell of self-interstitial-type defects. The geometrical correlation of defect formation is quite notable and is believed to play an important role in the clustering and diffusive evolution of the point defects. At high temperatures, it is believed that defect populations build up to *steady-state* values in time scales on the order of several seconds, thereby losing memory of the correlated formation. Little is known of the evolution during cascade aging, i.e. for time-scales on the order of several hundreds of picoseconds to several seconds. It is believed that the ultra fine-scale-microstructural

* Tel.: +1-805 893 3412; fax: +1-805 893 4731; e-mail: bdwirth@engineering.ucsb.edu.

[1] A few key references are only cited that are representative of a larger literature.

PII S0022-3115(96)00736-2

and microchemical evolution occurs through point-defect recombination, clustering, diffusion, trapping and annihilation at sinks.

Physically-based modeling of microstructural evolution under irradiation must be capable of accurately determining the fates of all solute and defect species for given combinations of irradiation and microstructural variables over the lifetime of the reactor pressure vessel, cf. 30 years. This requires the establishment of links—among a hierarchy of modeling techniques capable of treating temporal and spatial scales; these range from the picosecond and nanometer scale of the cascade evolution to the gigasecond and meter scale of the vessel lifetime [11]. Our approach is to develop a database of defect properties at the atomic scale as input into lattice kinetic Monte Carlo methods which treat defect evolutions during cascade aging; these in turn can provide input into kinetic rate theory approaches which can be directly compared to microstructural data, when available.

Outstanding questions regarding the nature of self-interstitial clusters in iron include both cluster morphology and mobility. The lack of observable interstitial loops in transmission electron microscopy (TEM) examination of neutron irradiated α-iron up to intermediate fluences of 2–5 $\times 10^{23}$ n/m^2 [12], as well as recent molecular-dynamics displacement cascade simulation results [8,10] raise the question of whether interstitial clusters form as faulted platelets (loops) or as three dimensional clusters. The lack of observable clusters in the TEM also raises the issue of possible high cluster mobility. Interstitial cluster mobility has profound significance to the kinetics of microstructural evolution: immobile clusters can serve as stable nuclei for interstitial-type loops, while mobile clusters diffuse to and are annihilated at sinks. For example, a population of clusters that anneal during irradiation mediate flux and temperature-dependent recombination rates.

In this paper, atomic-scale computer simulations are implemented in order to study systematically the structure, formation and migration properties of self-interstitials and small self-interstitial clusters, consisting of up to ten self-interstitial atoms, in α-iron. This is a first step toward detailed microscopic understanding and construction of a property database which is required to implement kinetic Monte Carlo methods for modeling cascade aging and irradiation-induced embrittlement in these steels over the wide range of time scales that characterize their microstructural evolution.

2. Simulation approach

Our atomic-scale simulations were based on a semi-empirical description of the interatomic interactions in α-iron according to the many-body potential-energy functions developed by Finnis and Sinclair [13], as modified recently by Calder and Bacon [8]. The dynamics of point-defect and self-interstitial cluster migration were investigated by isothermal–isobaric molecular-dynamics (MD) simulations using the MOLDY code [14]. Calculation of the self-interstitial and self-interstitial cluster formation energetics and structural characteristics was performed using a variant of the simulated annealing method based on isothermal–isobaric Metropolis Monte Carlo (MC) simulation in conjunction with steepest-descent quenching [15] as discussed below. In all of the simulations presented here, periodic boundary conditions were applied. The molecular-dynamics simulations of point defect and cluster migration were performed over the temperature range of 100 to 1000 K in simulation supercells with sizes ranging from $2000 + N$ to $8192 + N$ where N is the number of self-interstitial atoms in the supercell. In the calculations presented here, N is in the range of $1 \leq N \leq 10$.

To investigate the structure and energetics of self-interstitial clusters a relaxation schedule was employed consisting of 12 cooling stages at temperatures of 1050, 900, 800, 600, 400, 250, 150, 50, 10, 1, 0.1 and 0.01 K for each cluster size. At each cooling stage, the structure was equilibrated thermally by MC simulation at zero pressure. The resulting equilibrated configuration was mapped onto its corresponding local minimum-energy configuration by steepest-descent quenching; this quenched configuration provided the initial atomic configuration for repeating the procedure at the next cooling stage. The initial configuration of the first cooling stage for a cluster of N self-interstitial atoms consisted of N randomly oriented interstitial dumbbells about N neighboring lattice sites in a region around the geometrical center of the supercell. To ensure that the above relaxation procedure gave the ground-state configuration of the cluster, the procedure was repeated for several cluster sizes (N) starting with different higher-symmetry initial configurations, such as planar configurations with all interstitial dumbbells oriented in the same direction and lying on the same plane. Supercells that contained from $2000 + N$ to $8192 + N$ atoms were employed for the calculation of cluster structure and formation energetics. The different supercell sizes were used to ensure that strain interactions of the cluster due to the periodic boundary conditions were negligible.

3. Structure and energetics of self-interstitial clusters

The stable configuration for the single self-interstitial in α-iron was found to be the $< 110 >$ oriented split-interstitial dumbbell with a formation energy of 4.76 eV, in agreement with both previous atomistic simulations [8,16,17] and experiment [18]. Notably, two metastable configurations were found with respect to the stable configuration with formation energies less than 0.15 eV above that of the $< 110 >$ dumbbell. These two configurations are the $< 111 >$ oriented split-interstitial dumbbell, with a formation energy of 4.87 eV, and the crowdion configura-

tion with a formation energy of 4.91 eV. The relaxed atomic positions and formation energies are given in Table 1, along with those of the vacancy for comparison. The crowdion is the saddle point for migration of the $< 111 >$ dumbbell and can be considered to consist of 3 atoms sharing 2 lattice sites. The metastable configurations play a key role in the migration of the single interstitial, as discussed below.

The relative stability of the different self-interstitial configurations is consistent with previous work of Harder and Bacon [19] which was based on an earlier version of the N-body potential for α-iron. The formation volumes obtained in this study are somewhat larger than the formation volume of 1.33 Ω for the $< 110 >$ split-dumbbell quoted by Calder and Bacon [8]. However, the relaxed structure and properties of the $< 111 >$ split-dumbbell or crowdion configurations were not reported in that study. The formation energy and volume of the vacancy are in agreement with those previously published [17].

While the stable configuration of a single self-interstitial in α-iron is the $< 110 >$ oriented dumbbell, the stable configuration of clusters of two or more self-interstitials was found to consist of $< 111 >$ oriented dumbbells, with an increasing number of dumbbells being replaced by crowdions as the cluster size (N) increases. Fig. 1a shows the stable configuration of a 4-member self-interstitial cluster. The configuration consists of three dumbbells and one crowdion oriented along the $[11\bar{1}]$ direction, two of which lie on one (110) plane and the other two on an adjacent (110) plane; we call this relaxed structure a 2×2 configuration. The computed formation energy of this 2×2 configuration is 14.44 eV. The formation energies of the other possible 4-member cluster configurations were calculated to verify that the relaxation scheme employed resulted in the true ground-state energy. Fig. 1b shows a configuration with all of the four dumbbells lying on the same {110} plane, a 4×0 configuration, and Fig. 1c shows the atoms of three of the four dumbbells (or crowdions) lying on one {110} plane, while the fourth dumbbell lies on an adjacent {110} plane, a 3×1 configuration. The formation energies of the 4×0 and 3×1 configurations are 15.55 eV and 15.25 eV, respectively.

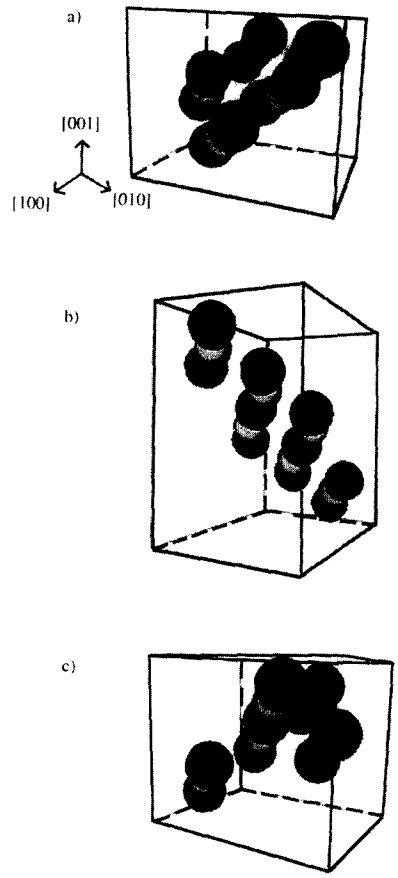

Fig. 1. Fully relaxed structure of self-interstitial clusters of size $N = 4$ in the (a) stable (2×2) configuration, (b) the planar (4×0) and (c) the (3×1). Vacant lattice sites and atoms displaced by more than 30% of the lattice parameter from their closest lattice site are denoted by light and dark gray colored spheres, respectively. In the split-interstitial dumbbell configurations, one lattice site (light) is shared by two atoms (dark), while in the crowdion configurations two lattice sites (light) are shared by three atoms (dark).

Table 1
Relaxed structure and formation properties of point-defects in α-iron [a]

Defect	Atomic positions (a)	Formation energy (eV)	Formation volume (Ω)
$< 110 >$ dumbbell	(0.245, 0.245, 0.5) (0.755, 0.755, 0.5)	4.76	1.43
$< 111 >$ dumbbell	(0.291, 0.291, 0.291) (0.709, 0.709, 0.709)	4.87	1.74
$< 111 >$ crowdion	(0.331, 0.331, 0.331) (0.749, 0.749, 0.749) (1.167, 1.167, 1.167)	4.91	1.77
vacancy		1.83	0.93

[a] Relaxed self-interstitial atomic positions are given in units of the lattice parameter, a, and formation volumes are given in units of atomic volume, Ω. The fully relaxed formation energy and volume of the vacancy are given for comparison.

The structural characteristics of the stable 4-member cluster demonstrated in Fig. 1 are generic characteristics for self-interstitial clusters with sizes over the range $2 \leq N \leq 10$. The minimum-energy cluster configurations consist of $< 111 >$ dumbbells and/or crowdions that lie on one, two, or more adjacent {110} planes and are oriented along $< 111 >$ directions. Furthermore, the number of crowdions in the stable cluster configuration increases with the cluster size. The cluster morphology appears to be

three-dimensional. The increasing number of crowdions in the clusters gives the impression of an extended defect configuration. For example, the stable configuration of a 9-member cluster consists of nine [111] crowdions situated on three adjacent $(01\bar{1})$ planes with three crowdions on each $(01\bar{1})$ plane. This fully relaxed structure of the 9-member cluster is shown in Fig. 2.

The cluster formation energy E^f is plotted in Fig. 3 as a function of the cluster size N. The results of Fig. 3 show the strong binding energy of the interstitial clusters. The slope of the $E^f(N)$ curve is approximately 3 eV per self-interstitial atom compared with the formation energy of 4.76 eV of a single $<110>$ self-interstitial dumbbell. The binding energy, E_N^b, for the last interstitial atom to a cluster of size N is given by:

$$E_N^b = \left(E_{N-1}^f + E_{<110>}^f\right) - E_N^f. \quad (1)$$

The binding energy E_N^b is 1.10 eV, 1.45 eV and 2.16 eV for $N = 2$, 3 and 4, respectively. The cluster binding energy as a function of cluster size is plotted in Fig. 4. As shown, the clusters are strongly bound, the binding energies are in excess of 1 eV and generally increase with increasing cluster size. The figure demonstrates that a 7-member cluster is the most strongly bound, and the nature of the binding energy curve suggests a geometrically preferred packing of the clusters which needs to be examined further.

The structural results for the 4-member cluster illustrated in Fig. 1 demonstrate that there exists a manifold of metastable configurations for an interstitial cluster of given size N within an energy range on the order of 1 eV above the cluster ground-state energy; these energy differences are smaller than the binding energy, E_N^b, of the cluster. Thus, a neutron displacement cascade depositing many keV of excess energy in a relatively small volume would be expected to generate self-interstitial clusters in metastable configurations at the initial stage (a few picoseconds) of its development; this is consistent with the results of recent MD simulations of the early stages of displacement cascade evolution in α-iron, employing primary knock-on atoms with energies on the order of 10 keV [8–10].

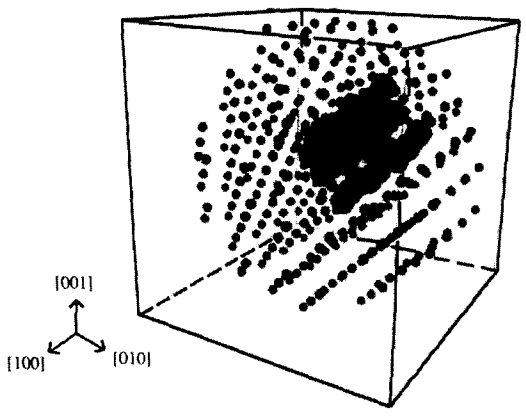

Fig. 2. Fully relaxed structure of self-interstitial cluster of size $N = 9$. Lattice atoms in their relaxed positions, vacant lattice sites, and atoms displaced by more than 30% of the lattice parameter from their closest lattice site are denoted by small dark, large light, and large dark gray colored spheres, respectively.

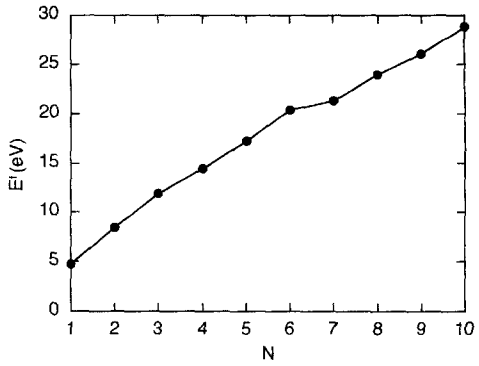

Fig. 3. Formation energy of self-interstitial clusters as a function of the cluster size N, where $N = 1$ corresponds to a single self-interstitial atom.

The three-dimensional morphology of the stable self-interstitial cluster structure is easily visualized as shown in Figs. 1 and 2. However, the possibility that the cluster has a dislocation loop morphology, as has been suggested in the literature [8,16,17] has also been examined. First, the two possible definitions of a dislocation loop in the context of an interstitial cluster must be considered. The first defines an interstitial dislocation loop as having all of the self-interstitial dumbbells (and/or crowdions) inhabiting a single plane. An example of such a configuration is shown in Fig. 5a and b and also was demonstrated in Fig. 1b for the 4-member cluster in the 4×0 configuration. Using this definition, it is impossible to conceive of the observed clusters being associated with a loop. The second possible

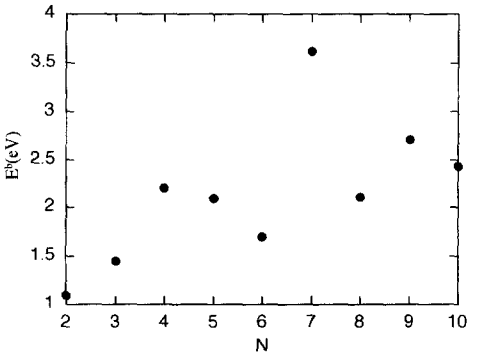

Fig. 4. Binding energy, Eq. (1), of self-interstitial clusters as a function of the cluster size N.

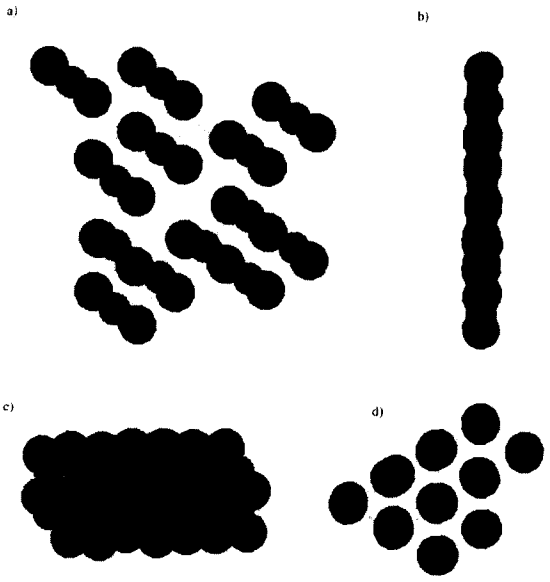

Fig. 5. (a) [$\bar{1}$01] projection of a planar self-interstitial cluster, (b) [101] projection of a planar self-interstitial cluster, (c) [0$\bar{1}$1] projection of a self-interstitial cluster dislocation loop and (d) [$\bar{1}$11] projection of self-interstitial dislocation loop. Vacant lattice sites and atoms displaced by more than 30% of the lattice parameter from their closest lattice site are denoted by light and dark gray spheres, respectively.

definition for an interstitial dislocation loop employs the center of mass of each of the self-interstitial dumbbells (or crowdions) that lie on a common plane as illustrated in Fig. 5c and d.

Fig. 6 shows two projections of the 7-member self-interstitial cluster. This cluster was chosen to demonstrate the possible existence of a loop morphology because it is the most strongly bound cluster; an example will also be given of the 10-member cluster. Fig. 6a and b show a [011] and [11$\bar{1}$] projection of the cluster. Clearly, the cluster is not consistent with either of the dislocation loop structures defined in Fig. 5. However, if some of the cluster crowdions are translated in the $< 111 >$ direction, as dynamically occurs during thermal oscillation or cluster migration, then it becomes possible to visualize the cluster as the dislocation loop that is shown in a [0$\bar{1}$1] projection in Fig. 5c. Such a 7-member cluster following appropriate $< 111 >$ translation of some of the crowdions is shown in [011] projection in Fig. 6c. Fig. 6d shows schematically the {110} planes from the projection of Fig. 6c; the extrinsic platelet of the crowdion cluster is clearly observed.

Fig. 7 shows similar projections for the 10-member cluster as it resulted following the structural relaxation, Fig. 7a and b, and following the $< 111 >$ translation of selected crowdions in Fig. 7c. Such a dislocation loop as shown by the self-interstitial clusters of Fig. 6c and Fig. 7c would be a perfect dislocation loop having a Burgers vector of $a/2[111]$ and as such would be expected to be glissile. The demonstrated loop morphology of the clusters is in agreement with previous work by Harder and Bacon [16] who used an earlier version of the N-body potential. Our study suggests that even if self-interstitial clusters appear as dislocation loops, they would nucleate with a Burgers vector of $a/2 < 111 >$ rather than nucleating with $a/2 < 110 >$ and subsequently transforming to a perfect loop through a shear transformation, as originally suggested by Bullough and Perrin [19] from simulations based on a pair potential.

We conclude that the morphology of self-interstitial clusters is highly complex. The lowest energy configurations observed for the clusters involve $< 111 >$ dumbbells and/or crowdions, with a predominance of crowdions with increasing cluster size N, which occupy adjacent {110} planes in a clearly extended, 3-dimensional arrangement. However, as discussed below, self-interstitial clusters are highly mobile with migration occurring along $< 111 >$ directions. It is, therefore, conceivable that a cluster could dynamically arrange itself into a compact dislocation loop configuration with a Burgers vector $\boldsymbol{b} =$

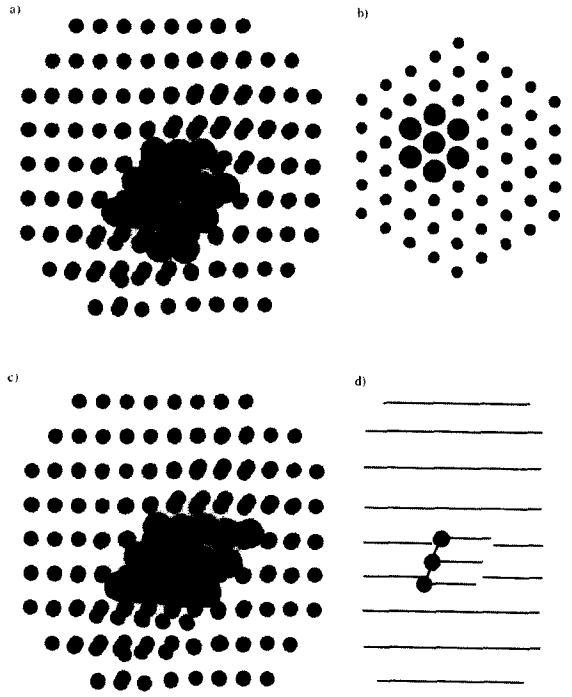

Fig. 6. (a) [011] projection of the fully relaxed 7-member self-interstitial cluster, (b) [11$\bar{1}$] projection of the cluster, (c) [011] projection following $< 111 >$ translation of selected cluster crowdions and (d) schematic representation of the {110} planes in the translated cluster. Lattice atoms in their relaxed positions and atoms displaced by more than 30% of the lattice parameter from their closest lattice site are denoted by small dark and large dark gray spheres, respectively.

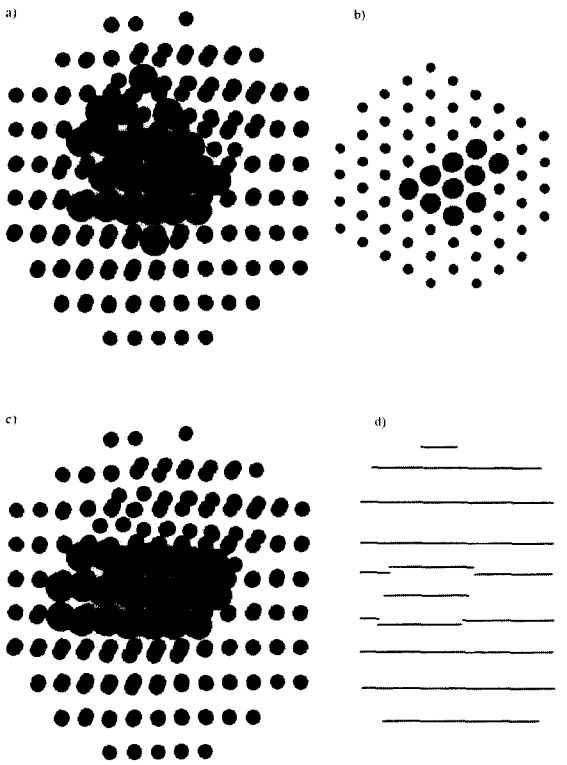

Fig. 7. (a) $[01\bar{1}]$ projection of the fully relaxed 10-member self-interstitial cluster, (b) $[\bar{1}11]$ projection of the cluster, (c) $[01\bar{1}]$ projection following $< 111 >$ translation of selected cluster crowdions and (d) schematic representation of the {110} planes in the translated cluster.

$a/2 < 111 >$ during thermal oscillation, migration, or perhaps even at its birth in the cascade where a high density of excess energy is deposited.

4. Mobility of self-interstitials and self-interstitial clusters

Molecular-dynamics simulations of self-interstitial migration were performed over the temperature range of 100 K $\leq T \leq$ 1000 K. Visualization of the simulation results led to the observation that self-interstitial migration in α-iron is a *two-step* process. Using the migration path observed in molecular-dynamics simulations at $T = 250$ K as a guide, molecular-statics simulations along the migration-path coordinate were performed to obtain a more quantitative picture of the barriers for the observed mechanisms. Fig. 8 shows a semi-quantitative picture of the two migration mechanisms and the magnitude of the energy barriers involved.

Based on our calculations, we conclude that self-interstitial migration in α-iron involves two mechanisms. A rotation from the $< 110 >$ to a $< 111 >$-oriented dumbbell and then a translation of the dumbbell along the $< 111 >$ direction. Once the self-interstitial has rotated into the $< 111 >$ split-dumbbell configuration, it can make one or more translational jumps along $< 111 >$ before rotating back to the lowest-energy $< 110 >$ split-dumbbell configuration. The $< 111 >$ translation has a very low energy barrier of 0.04 eV, i.e. it is practically an athermal migration process, while the rotation from $< 110 >$ to a $< 111 >$ dumbbell has an energy barrier of approximately 0.25 eV.

The nature of the energy barriers for translation and rotation has profound effects on the kinetics of self-interstitial migration. Self-interstitials created as $< 111 >$ dumbbells would be expected to migrate even at very low temperatures by translation until annihilation or rotation into a $< 110 >$ configuration. Self-interstitials created as $< 110 >$ dumbbells would be stable at low temperatures,

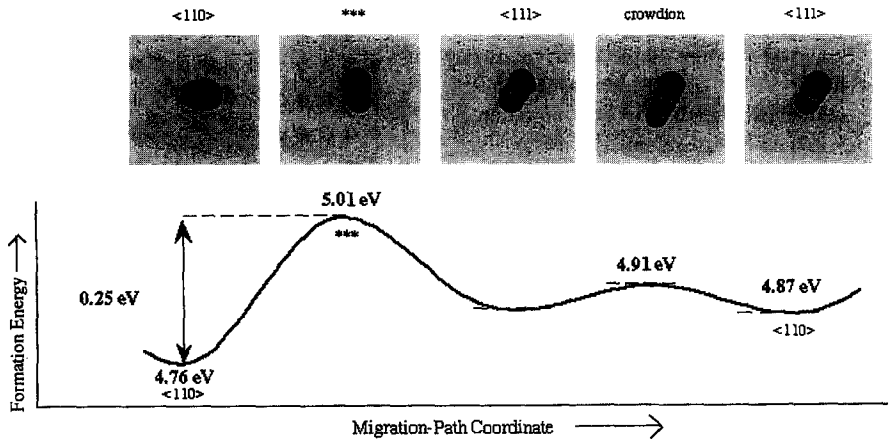

Fig. 8. Energetics of self-interstitial migration as a function of the migration-path coordinate. The self-interstitial configurations shown were obtained from molecular-dynamics simulation at $T = 250$ K and were relaxed fully for constructing this semi-quantitative plot.

require thermal activation to rotate to the $< 111 >$ configuration, and become mobile by translation in the $< 111 >$ direction until the self-interstitial either annihilates with a vacancy-type defect, clusters with other self-interstitial defects, or rotates back into the $< 110 >$ configuration.

Molecular-dynamics simulations of self-interstitial cluster migration with cluster sizes $N = 2$, 3 and 4 were performed over the temperature range 100 K $\leq T \leq$ 1000 K for times up to 100 picoseconds. In addition, an 11-member cluster which absorbs an interstitial at 550 K was simulated for 100 picoseconds. Although further simulations are required to provide a determination of the temperature dependence of cluster migration, the results presented here provide a qualitative picture of the migration mechanisms for such clusters. For each of the self-interstitial clusters that were simulated, $N = 2$, 3, 4, 11 and 12, migration occurred by collective $< 111 >$ translations along the $< 111 >$ orientation direction of the dumbbells and/or crowdions in the cluster by the 'local' dissociation and reassociation of interstitials to the cluster in an amoeba-like fashion. Complete dissociation of an interstitial from a cluster was not observed nor is it expected due to the high magnitude of their binding energy, as discussed above.

Fig. 9 shows molecular-dynamics snapshots of a migrating di-interstitial ($N = 2$) at $T = 560$ K as viewed from a single projection. As shown, the cluster consists of parallel $< 111 >$ dumbbells which occupy third-nearest neighbor positions. In Fig. 9a–c, cluster migration through the crowdion mechanism is shown. Between Fig. 9c and d, the cluster rotates to a new $< 111 >$ direction before continuing its translation along the newly oriented $< 111 >$ in Fig. 9e and f. It is notable that this simulation of the two-member cluster migration at $T = 560$ K is the only case in which a self-interstitial cluster has been observed to rotate from one $< 111 >$ direction to a different $< 111 >$ direction.

Fig. 10 shows a similar series of snapshots for a four-member cluster, in the 2×2 ground-state configuration at $T = 550$ K. In similar manner with the di-interstitial, net cluster migration occurs by the collective $< 111 >$ translation of the dumbbells and crowdions. It is notable that the cluster is capable of traveling large distances along the $< 111 >$ orientation direction and that the migration is highly anisotropic and one-dimensional. In simulations we have performed to date, the cluster trapping found in a long time cascade simulation performed by Stoller [10] was not observed. However, an extensive investigation of cluster migration with other defects present in the simulation supercell remains to be examined further.

Our molecular-dynamics simulations over a wide temperature range make possible a qualitative comparison of the migration of the 4-member cluster to that of a single interstitial in α-iron. The net mean-squared displacement of the center of mass of a 4-member self-interstitial cluster

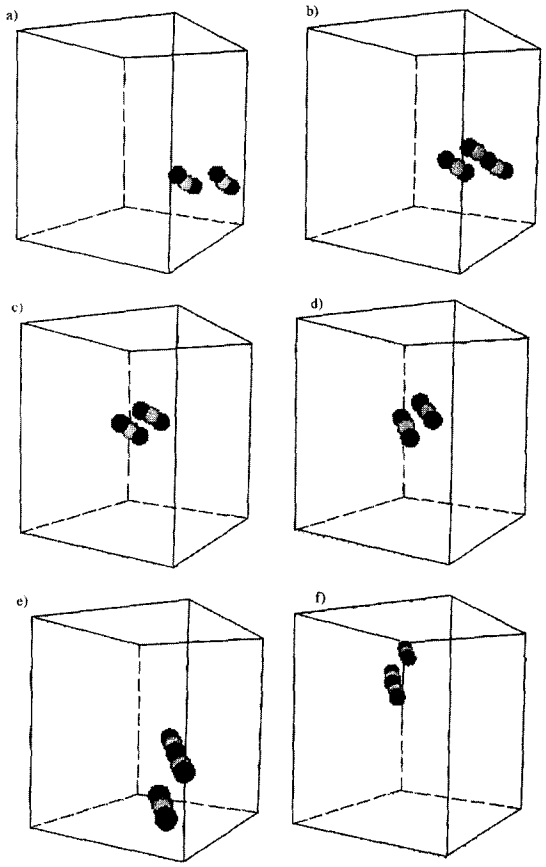

Fig. 9. Snapshots of di-interstitial migration at $T = 560$ K. The di-interstitial rotates from one $< 111 >$ direction to another between frames (c) and (d). Elapsed time is (a) 0, (b) 0.9 ps, (c) 2.6 ps, (d) 3.0 ps, (e) 5.6 ps and (f) 11.4 ps.

over the temperature 250 K $\leq T \leq$ 1000 K was found to be of the same magnitude as for a single self-interstitial when normalized by the simulation time. It should be noted that migration of the 4-member cluster has only been observed to occur by the single mechanism of co-ordinated $< 111 >$ translations, while the single self-interstitial migrates by a two-step process, thus the overall kinetics can not be compared exactly. However, the qualitative conclusion that the energy barrier, E_N^m, to migration of small self-interstitial clusters is of the same order of magnitude as that of the single interstitial; an estimate that E_N^m is on the order of 0.1 eV has been justified. An important conclusion is that for $N = 4$, E_N^m is significantly lower than the binding energy of the cluster which exceeds 2 eV.

For $N = 4$, dynamic simulations of two different cluster configurations, the 4×0 and the 2×2 configuration, have been performed both with and without sinks (vacancy loops and free surfaces) present in the supercell with no observable difference in the migration mechanism. Additionally, a molecular-dynamics simulation at $T = 560$ K of a larger cluster ($N = 11$) which grew (to $N = 12$) by the absorption of an interstitial displayed the same migration

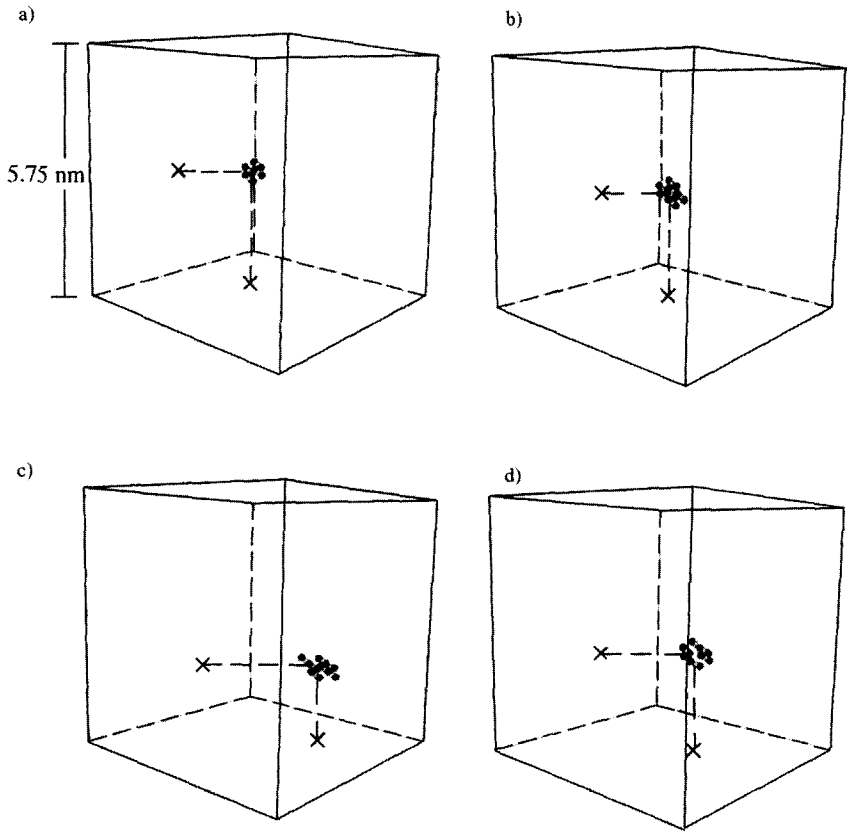

Fig. 10. Snapshots of a 4-member interstitial cluster migration at $T = 550$ K. Elapsed time is (a) 0 ps, (b) 2.8 ps, (c) 9 ps and (d) 25 ps.

process. Therefore, to within the accuracy of the interatomic potential used in our simulations, we conclude that self-interstitial clusters with $N > 10$ will consist of $< 111 >$ dumbbells arranged in a '3-dimensional' configuration on adjacent {110} planes and will rapidly migrate in an anisotropic manner along their $< 111 >$ axis. However, the possibility of cluster trapping or migration blockage has not yet been examined.

5. Discussion

An argument has long existed as to whether the defect production and annealing kinetics were best described in terms of a one or a two-interstitial model [20,21]. Briefly, the one interstitial model attributes the formation of self-interstitial defects to a single population in the ground-state configuration which recovers during annealing (in stage I) by the migration of the ground-state self-interstitial. In contrast, the two-interstitial model describes self-interstitial formation in terms of a population of interstitials formed in either the ground-state configuration or a metastable configuration which recovers by migration of the metastable interstitial (in stage I) and ultimately a migration of the ground state configuration (stage III). In the two-interstitial model, it is expected that migration of the metastable configuration will occur at much lower temperatures, i.e. lower migration energy, than the ground-state interstitial. The one-interstitial model ascribes vacancy migration to stage III recovery while the two-interstitial model does not provide for vacancy migration until stage V recovery. The one-interstitial model has become the accepted model for interpreting the defect production and annealing kinetics. The simulation results presented here, which detail a two-step migration process involving the metastable $< 111 >$ split-dumbbell and crowdion configurations, suggest that perhaps this debate should be revisited.

The atomistic simulation results provide insight into modeling the production and mobility of single self-interstitial defects. Kinetic rate theory approaches can be used to describe the populations of $< 110 >$ and $< 111 >$ split-dumbbells, as well as those of crowdions. Quantitative details of the energy barriers for rotation in and out of the ground state can be obtained from molecular-statics simulations along the corresponding migration-path coordinates, while the numbers and configurations produced

during displacement cascades could be obtained from the cascade modeling. Thus, the annealing and cascade aging behavior of self-interstitial populations can be modeled quantitatively.

The lack of observable dislocation loops in the TEM following neutron irradiations to low to intermediate fluences has been a long-standing puzzle to the irradiation damage community. The simulation results presented here suggest that the reason may be two-fold. First, the stable morphology of small self-interstitial clusters is an extended three-dimensional cluster. Such a configuration may enable a much higher interstitial density in a volume still below the TEM resolution. Second, and perhaps more important, is the cluster mobility. The simulation results presented here suggest that such clusters are very mobile even at relatively low temperatures and thus, it is expected that the interstitial clusters formed during irradiation would rapidly migrate to and annihilate at sinks in the system.

It is still unknown what effect solute impurities may have on the morphology and mobility of interstitial clusters. It is conceivable that mobile clusters would be effectively trapped by solute atmospheres — especially with respect to interstitial-type solutes such as C, P and N which might naturally be expected to form complexes with the clusters due to strain field interactions. However, clarification of these issues remains a subject for further study.

The strong angular dependence of bonding in transition metals, such as α-iron, is not accounted for in the semi-empirical potential [8,13] used in this study. The extent to which such many-body angular forces will impact the structural characteristics and migration behavior of self-interstitial defects is not clearly known. Recent calculations by Xu and Moriarty on molybdenum [22] found that the self-interstitial formation and migration energies were increased over those predicted by the Finnis–Sinclair interatomic potential; the relative stability, however, of the different configurations remained unchanged. Thus the quantitative validity of the simulation results presented here should be accepted to within the limitations of the Finnis–Sinclair potential employed.

6. Summary

We have presented the results of a comprehensive atomistic study of the structure and formation and migration energetics of the self-interstitial and small ($N = 2$–10) self-interstitial clusters in α-iron. Our atomic-scale study was based on a combination of molecular-dynamics and structural relaxation simulations using a Finnis–Sinclair-type potential for the description of the interatomic interactions. The structural relaxation procedure has revealed that the stable cluster configurations are highly complex 3-dimensional structures consisting of $< 111 >$ oriented dumbbells and/or crowdions which occupy adjacent {110} planes. Molecular-dynamics simulations over a wide temperature range have revealed that single interstitial migration is a two-step process involving rotations out of and into the ground-state $< 110 >$ dumbbell configuration and translation of $< 111 >$ dumbbells through the crowdion saddle-point configuration. Self-interstitial clusters are highly mobile and they migrate in a highly anisotropic, one-dimensional manner along their $< 111 >$ orientation. These results provide insight into the microstructural evolution which occurs under irradiation in pressure vessel steels, especially in explaining the lack of observable dislocation loops in TEM examinations of such steels.

References

[1] G.R. Odette, P.M. Lombrozo and R.A. Wullaert, in: Proc. Conf. on Effects of Radiation on Materials, ASTM STP 870, ed. F.A. Garner and J.S. Perrin, ASTM STP-870 (American Society for Testing and Materials, Philadelphia, 1985) p. 840.
[2] W.J. Phythian and C.A. English, J. Nucl. Mat. 205 (1993) 162.
[3] F. Frisius, R. Kampmann, P.A. Beaven and R. Wagner, in: Proc. Conf. on Dimensional Stability and Mechanical Behavior of Irradiated Metals and Alloys (BNES, London, 1983) p. 171.
[4] G.R. Odette, Scripta Metal. 17 (1983) 1183.
[5] G.R. Odette and G.E. Lucas, in: Proc. Conf. on Radiation Embrittlement of Nuclear Reactor Pressure Vessel Steels, ASTM STP909, ed. L.E. Steele, ASTM STP-909 (American Society for Testing and Materials, Philadelphia, 1986) p. 206.
[6] G.R. Odette, E.V. Mader, G.E. Lucas, W.J. Phythian and C.A. English, in: Proc. Conf. on Effects of Radiation on Materials, ASTM STP 1175, ed. A.S. Kumar, D.S. Gelles, R.K. Nanstad and E.A. Little, ASTM STP-1175 (American Society for Testing and Materials, Philadelphia, 1993) p. 373.
[7] M.T. Robinson, J. Nucl. Mater. 216 (1994) 1.
[8] A.F. Calder and D.J. Bacon, J. Nucl. Mater. 207 (1993) 25.
[9] W.J. Phythian, R.E. Stoller, A.J.E. Foreman, A.F. Calder and D.J. Bacon, J. Nucl. Mater. 223 (1995) 245.
[10] R.E. Stoller, in: Proc. Conf. Symp. on Microstructure of Irradiated Materials, MRS, ed. I.M. Robertson, L.E. Rehn, S.J. Zinkle and W.J. Phythian (Materials Research Society, Pittsburgh, 1995) p. 21.
[11] G.R. Odette, in: IAEA Tech. Rep. Ser., Vienna, in press.
[12] M.L. Jenkins, M.A. Kirk and W.J. Phythian, J. Nucl. Mater. 205 (1993) 16.
[13] M.W. Finnis and J.E. Sinclair, Philos. Mag. A 50 (1984) 45.
[14] M.W. Finnis, MOLDY 6 – A Molecular Dynamics Program for Simulation of Pure Metals, UKAEA Harwell Laboratory, AERE R-13182 (1988).
[15] D. Maroudas and R.A. Brown, Phys. Rev. B 47 (1993) 15562.
[16] J.M. Harder and D.J. Bacon, Philos. Mag. A 58 (1988) 165.
[17] R. Bullough and R.C. Perrin, Proc. Roy. Soc. Lond. A 305 (1968) 541.

[18] P. Ehrhart, K.H. Robrock and H.R. Schober, Physics of Radiation Effects in Crystals, MPCMS Vol. 13 (North-Holland Physics, Amsterdam, 1986).
[19] J.M. Harder and D.J. Bacon, Philos. Mag. A 54 (1986) 651.
[20] W. Schilling, P. Erhart and K. Sonnenberg, in: Fundamental Aspects of Radiation Damage in Materials, CONF-751006-P1, Vol. 1, ed. M.T. Robinson and F.W. Young, Jr. (1975) p. 470.
[21] A. Seeger, in: Fundamental Aspects of Radiation Damage in Materials, CONF-751006-P1, Vol. 1, ed., M.T. Robinson and F.W. Young, Jr. (1975) p. 493.
[22] W. Xu and J.A. Moriarty, Phys. Rev. B 54 (1996) 6941.